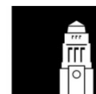

UNIVERSITY OF LEEDS

This is a repository copy of *Negative differential resistance in direct bandgap GeSn p-i-n structures*.

White Rose Research Online URL for this paper:
http://eprints.whiterose.ac.uk/89357/

Version: Accepted Version

Article:

Schulte-Braucks, C, Stange, D, Von Den Driesch, N et al. (5 more authors) (2015) Negative differential resistance in direct bandgap GeSn p-i-n structures. Applied Physics Letters, 107 (4). 042101. ISSN 0003-6951

https://doi.org/10.1063/1.4927622

Reuse

Unless indicated otherwise, fulltext items are protected by copyright with all rights reserved. The copyright exception in section 29 of the Copyright, Designs and Patents Act 1988 allows the making of a single copy solely for the purpose of non-commercial research or private study within the limits of fair dealing. The publisher or other rights-holder may allow further reproduction and re-use of this version - refer to the White Rose Research Online record for this item. Where records identify the publisher as the copyright holder, users can verify any specific terms of use on the publisher's website.

Takedown

If you consider content in White Rose Research Online to be in breach of UK law, please notify us by emailing eprints@whiterose.ac.uk including the URL of the record and the reason for the withdrawal request.

eprints@whiterose.ac.uk
https://eprints.whiterose.ac.uk/

Negative differential resistance in direct bandgap GeSn p-i-n structures

C. Schulte-Braucks, D. Stange, N. von den Driesch, S. Blaeser, S. Mantl, and D.Buca
Peter Grünberg Institut (PGI-9), Forschungszentrum Jülich and JARA, 52425 Jülich, Germany
Z. Ikonic
Institute of Microwaves and Photonics, School of Electronic and Electrical Engineering, University of Leeds, Leeds LS2 9JT, United Kingdom
J.M. Hartmann
University of Grenoble Alpes, F-38000 and CEA, LETI, MINATEC Campus, F-38054 Grenoble, France

(Dated: 24 May 2015)

Certain GeSn alloys are group IV direct bandgap semiconductors with prospects for electrical and optoelectronical applications. In this Letter we report on the temperature dependence of the electrical characteristics of high Sn-content $Ge_{0.89}Sn_{0.11}$ *p-i-n* diodes. NiGeSn contacts were used to minimize the access resistance and ensure compatibility with silicon technology. The major emphasis is placed on the negative differential resistance in which peak to valley current ratios up to 2.3 were obtained. TCAD simulations were performed to identify the origin of the various current contributions, providing evidence for direct band to band tunneling and trap assisted tunneling.

The recent experimental proof of GeSn as group IV direct bandgap semiconductor[1] will stimulate novel applications in photonics and electronics. Due to its low direct bandgap energy and silicon compatibility GeSn alloys are particularly interesting for tunneling field-effect transistors (TFETs) for ultra-low power electronics[2,3]. *p-i-n* diodes are the basic building blocks of tunneling-FETs enabling band-to-band tunneling allowing the extraction of material parameters such as tunneling masses[4]. Since the first demonstration of a tunneling diode by Leo Esaki[5] showing the characteristic negative differential resistance tunneling diodes have been fabricated with different indirect group IV semiconductors such as Si[6], Ge[7] & SiGe[8]. However, the highest tunneling current densities were achieved on direct, low bandgap III-V semiconductors, like InAs[9], adding sustained effort for integrating III-V semiconductors on Si wafers. Recently developed GeSn alloys with Sn contents above 10% provide new perspectives for Si electronics by combining the advantages of III-V compounds as low effective mass of Γ-electrons and the direct bandgap with state-of-the-art Si platform technology. Several papers on GeSn MOSFETs[10,11] and even TFETs[2,12] have demonstrated that GeSn alloys can be technologically integrated. However, these devices had low Sn-contents below the indirect to direct transition.

In this Letter we present the fabrication and electrical characterization of direct bandgap group IV *p-i-n* diodes with emphasis on band-to-band tunneling (BTBT). First we address intrinsic material properties, as bandgap and effective masses, obtained by calculations followed by the electrical characterization of Esaki tunneling diodes. Finally, the experimental results are compared with device simulations.

GeSn alloys pseudomorphically grown on Ge are under high biaxial compressive strain and thus are indirect semiconductors even with Sn contents of 10 %. By reducing the compressive strain, e.g. by growing thicker layers, the Γ-valley decreases faster in energy than the L-valley and GeSn becomes a direct semiconductor[13]. Fig.1(a) depicts the calculated bandgap vs. compressive strain pointing out the necessity of strain relaxation for achieving direct bandgap GeSn. The strain at which this transition takes place depends on the Sn content and for $Ge_{0.89}Sn_{0.11}$, relevant in this work, is about -0.8% (Fig.1(a)). In addition to the advantage of a direct bandgap, GeSn layers offer also smaller effective masses for both, holes and electrons[14], suggesting themselves for tunneling based devices as TFETs[14]. The heavy hole (HH), light hole (LH) and the Γ-valley electron masses in-plane [100] and out of plane [001] direction as calculated with the 8×8 k · p method including strain[15] are plotted in Fig.1(b,c) for a set of Sn contents. The HH mass in tunneling direction [001] is independent of strain and decreases only slightly from $0.221\,m_0$ to $0.219\,m_0$ when the Sn-content changes from 9% to 12%, respectively. Here strain relaxation is beneficial as well enabling small tunneling masses and consequently high BTBT-rates. Independent off the directness ($E_L - E_\Gamma$) of the GeSn alloys compressive strain splits the valence band such that the HH becomes higher in energy. The Γ-HH and Γ-LH transition are both direct tunneling processes, without any change of the in-plane wave-vector $k_\parallel$. However, due to $p_{x,y}$-symmetry of HH wave-functions, and s-symmetry of conduction bands wave-functions the tunneling is not possible at $k_\parallel = 0$, but it sets in as $k_\parallel$ increases, due to band-mixing. The Γ-LH tunneling is possible even for $k_\parallel = 0$. Important factors influencing the tunneling current are Γ and L densities of states (DOS) defining the population of the electronic states. This is shown in Fig,1(d) as a function of temperature for different doping levels. The Γ-electron density increases with decreasing temperature, as electrons condensate into the lowest energy levels, but their fraction becomes lower with increasing doping: it is 100% for a total electron density of $1 \cdot 10^{17}\,cm^{-3}$ but it decreases to just 32% for $10^{18}\,cm^{-3}$

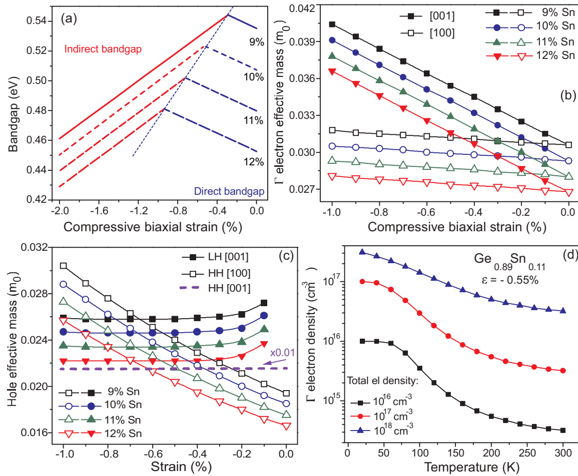

FIG. 1. Calculated (a) Bandgap, (b) Γ-electron effective mass and (c) lowest hole effective masses for GeSn alloys with Sn contents between 9% and 12% as function of biaxial compressive strain. (d) Γ-valley population for $Ge_{0.89}Sn_{0.11}$ under compressive strain of -0.55% for different n-type doping.

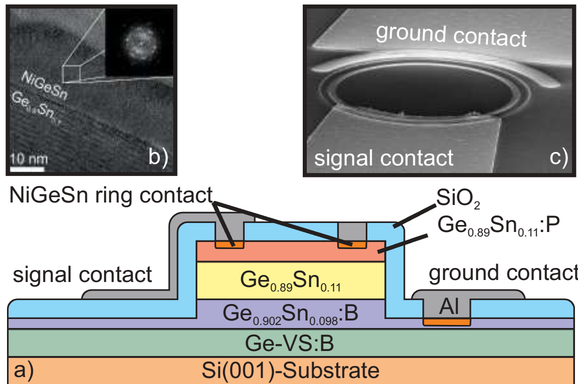

FIG. 2. GeSn *p-i-n* diode: a) device sketch; b) TEM micrograph of NiGeSn on GeSn showing a smooth interface and a well oriented NiGeSn as can be seen by the FFT-inset; c) SEM-image of a fabricated *p-i-n* diode

total electron density. The remaining electrons reside in the L-valley. Table I summarizes the material parameters at 300 K for the alloys discussed in this letter. These values are later used in TCAD simulations of the tunneling diodes.

Epitaxial growth of the GeSn layer stack was performed in an industry-compatible 200 mm AIXTRON TRICENT® reduced pressure chemical vapor deposition (CVD) reactor. Precursors as Ge_2H_6 and $SnCl_4$ enable the growth of GeSn alloys at temperatures of about 350 °C without undesired Sn segregation and surface precipitations[3,16]. For a high quality of the GeSn alloys and an easier device fabrication, the complete *p-i-n* layer stack was grown on a 2.5 μm thick highly p^+-doped[17] (B, $2 \cdot 10^{19}$ cm^{-3}) Ge virtual substrate (Ge-VS). The latter was grown on Si(001) using GeH_4 and B_2H_6 grown on Si(001)[17]. In order to avoid implantation induced damage, *in-situ* doped p^+ and n^+ type doped GeSn layers were epitaxially grown using B_2H_6 and PH_3, respectively. The electrically active carrier concentrations in the doped GeSn layers was about $2 \cdot 10^{19}$ cm^{-3} in the bottom 50 nm GeSn layer (B, p-type) and $1 \cdot 10^{20}$ cm^{-3} (P, n-type) in the top 80 nm GeSn alloy as determined by electrochemical capacitance-voltage (ECV) profiling. The scope of this letter is to show band-to band tunneling in a direct bandgap alloy. To that end, the GeSn layers are grown thicker than the critical thickness for plastic relaxation in order to promote strain relaxation and thereby realize an indirect to direct bandgap transition. The residual compressive strain in the partially relaxed $Ge_{0.89}Sn_{0.11}$ alloy is -0.55%.

GeSn *p-i-n* diodes were processed applying standard CMOS technology like reactive ion etching (RIE), optical lithography and NiGeSn contacts. However in order to avoid Sn diffusion low temperature process modules, below 325 °C have been developed. A sketch of the device and the layer stack is shown in Fig.2(a). First a 250 nm deep mesa was etched by RIE in order to contact the highly p-doped bottom layer. The following steps were SiO_2 passivation by plasma enhanced chemical vapour deposition, contact window opening by RIE and NiGeSn metal contact formation. As can be seen in Fig.2(b) the NiGeSn forms a smooth semiconductor-metal interface. The formation of the low resistive well oriented NiGeSn contact has been previously studied[18] and will not be discussed here any further. The fabrication completes with deposition of 200 nm thick Al bonding pads. Fig.2(c) depicts a SEM image of the fabricated device.

Temperature dependent I-V characteristics of a *p-i-n*-diode with a diameter of 50 μm are shown in Fig.3(a). A distinct region of negative differential resistance is observed for temperatures below 175 K. Three different regimes, typical for Esaki diodes, can be identified. i) band-to-band tunneling ii) excess current due to trap assisted tunneling (TAT) and iii) drift-diffusion by thermal emission of carriers over the potential barrier. For strong reverse bias the current only slightly increases with temperature. This is a typical behavior for direct band-to-band tunneling where no phonons are required for momentum conservation[4]. Here the band-to-band tunneling rate increases as the bandgap decreases with increasing temperature. The situation is different for slightly positive voltages below the peak-current voltage where BTBT is still dominant but the band overlap of conduction and valence bands of the n and p-type regions is small. Here the current increases with decreasing temperature which can be explained as follows. The energy separation of the Γ and L-valleys in the present layer structure is very small, about 13 meV. Consequently both, the Γ and L-valleys are populated at 300 K (Fig.1(d)). By decreasing the temperature electrons condensate into the Γ-valley. As the BTBT-probability for direct tunneling is much higher than for indirect tunneling the increased Γ-population leads to an increased tunneling current for lower temperatures at low bias (Fig.3(b)). A further in-

TABLE I. Material parameters of GeSn alloys grown on a Ge-VS under slight tensile strain of 0.15%, obtained by 8x8 k · p method. The Ge-VS top valence band defines the zero energy. Energies in (eV), masses in (m_0); l=[001] & t=[100] direction.

x_{Sn}	ϵ	E_{HH}	E_{LH}	E_{Γ}	E_{L}	m_{LHt}	m_{LHl}	m_{HHt}	m_{HHl}	$m_{\Gamma\mathrm{t}}$	$m_{\Gamma\mathrm{l}}$	m_{Ll}	m_{Ll}
0.11	-0.55%	0.131	0.079	0.638	0.651	0.046	0.022	0.023	0.220	0.029	0.033	1.559	0.08
0.098	-0.37%	0.109	0.073	0.640	0.648	0.050	0.022	0.025	0.221	0.030	0.033	1.559	0.08

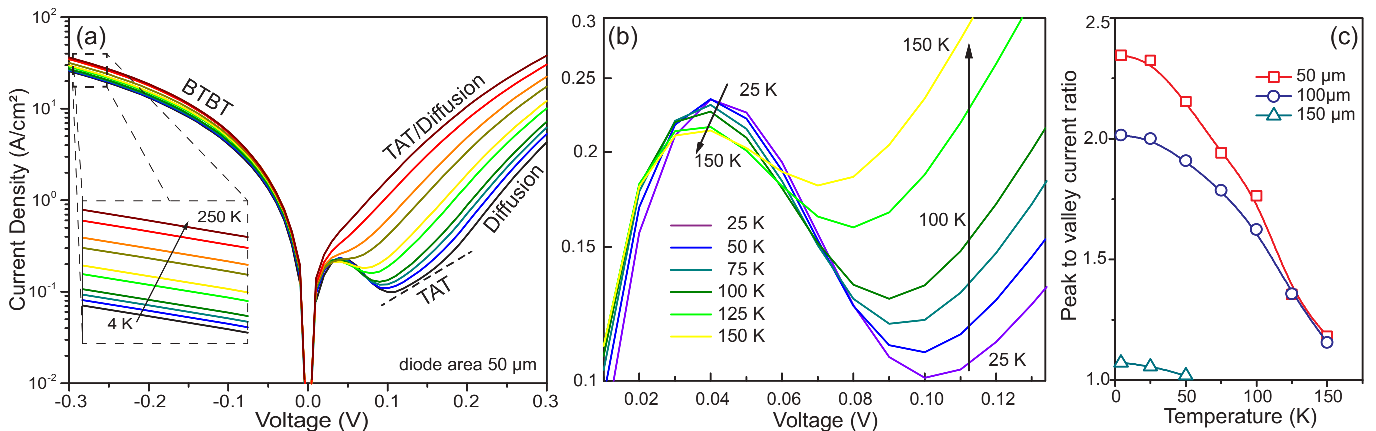

FIG. 3. (a) I-V characteristics of a *p-i-n* diode with 50 μm diameter showing NDR for $T < 175$ K. (b) zoom of the NDR region indicating the temperature dependence of the current components; (c) PVCR for different diode sizes plotted against the temperature. The PVCR depends almost linear on the temperature.

crease of the applied voltage suppresses the BTBT as conduction band of the n-type region and valence band of the p-type region do not overlap anymore (Fig.4(a)) resulting in a decrease of the current and giving rise to a negative differential resistance (NDR). Peak to valley current ratios (PVCR) of 2.3 and ~ 2 have been measured at 4 K for diodes with 50 μm and 100 μm diameters, respectively. Above 0.1 V, the BTBT is overlapped by trap assisted tunneling (TAT) that strongly depends on temperature and causes an excess current. As a consequence the valley current increases with temperature leading to a typical roughly linear dependence of the PVCR on temperature[8] (Fig. 3(c)). For larger forward biases thermal emission over the *p-i-n* junction barrier comes into play. The low bandgap value of 0.5 eV leads to a strongly enhanced diffusion current. Furthermore, as the (pseudo) intrinsic region is fairly large the BTBT probability is small in moderate forward bias. Thus, above 175 K diffusion and TAT currents dominate and NDR vanishes. To analyze the physical mechanisms simulations using a non-local BTBT model of the TCAD simulator Synopsis Sentaurus Device were performed. The input material parameters are summarized in Table I. The calculated real-space band structure of the *p-i-n* diode for different applied voltages is shown in Fig.4(a), indicating clearly a conduction band to valence band overlap of roughly 0.14 eV at zero bias which is crucial for achieving NDR. The simulated Esaki diode characteristics for 300 K are shown in Fig. 4(c). It should be pointed out that although Γ- and L-valleys have nearly the same energy, and the L-valley DOS is larger than for the Γ-valley, the contribution of direct BTBT is ~ 1000 times higher than indirect BTBT due to the significant differences in the effective masses and no-phonon involvement. At 300 K, in forward bias the strong contribution of diffusion current is masking the NDR effect. As the simulation takes into account Shockley-Read-Hall generation/recombination but not TAT the NDR is visible at higher temperatures than found experimentally. The voltage region of the NDR and the current density values are in good agreement with the experimental data. Further analysis revealed the contributions of BTBT and TAT by comparing different diode sizes. The fabricated *p-i-n* diodes feature ring contacts instead of classical circular contacts, suitable for light emitting diodes based on the direct bandgap of the $Ge_{0.89}Sn_{0.11}$ alloy. The analyses of the I-V characteristics for different diode sizes, Fig.5, indicates as expected that the current in reverse bias scales with the top NiGeSn ring contact area rather than with the circular area of the diode. In reverse bias BTBT dominates and scales with the junction area. However, in forward bias TAT dominates which does not scale with the contact area. This is also reflected in Fig.3(c) showing the PVCR for different temperatures and diode diameters. For larger diodes the PVCR is smaller and the NDR vanishes at lower temperatures indicating that the contribution of TAT is more pronounced for larger diodes. Point defects are typically incorporated in epitaxial layers grown at lower temperatures, here 350 °C, and presumably the main source of TAT. Optimized GeSn *p-i-n* structures with a thinner

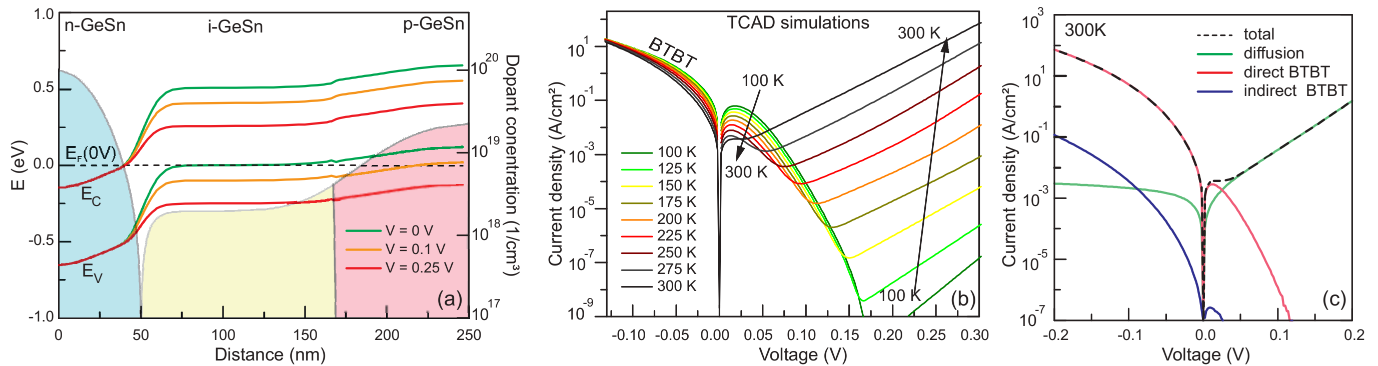

FIG. 4. (a) Electronic band structure alignment of the GeSn p-i-n diode at $T = 300\,\text{K}$. The doping profile as obtained by ECV is also indicated (right scale). (b,c) Simulated I-V Esaki diode characteristics: (b) temperature dependence and (c) current components at 300 K.

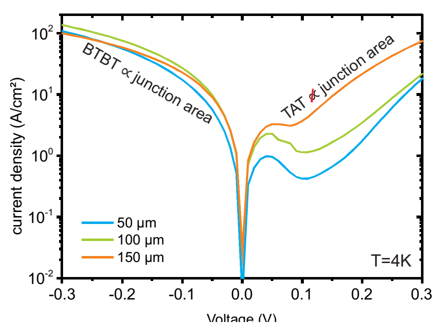

FIG. 5. Esaki diode characteristics for different diode sizes normalized by the area of the top ring electrode. In reverse bias, dominated by BTBT, the I-V curves overlap for different diode sizes as the BTBT-current scales with the junction area. In forward bias TAT is dominating which does not scale with the junction area.

intrinsic region, improved doping profiles and even lower bandgap are expected to increase the tunneling currents and to reach higher temperature NDR.

In conclusion, we have presented the characterization of GeSn tunneling diodes as a function of temperature. The BTBT current in the direct bandgap $Ge_{0.89}Sn_{0.11}$ diodes scales with the contact area. An NDR effect with a PVCR up to 2.3 has been achieved at low temperatures. The appearance of TAT is attributed to point defects which may stem from the ultralow temperature CVD growth. Band-structure and device simulations provided deeper insight in the benefit of direct tunneling even for only slightly direct GeSn alloys due to small effective masses. Further analysis of GeSn tunneling diodes will provide important data such as tunneling masses. The realization of Esaki type GeSn represents an important step towards advanced Si-based tunneling-FETs.

This research received partial funding from the European Community's Seventh Framework Programme (grant agreement no. 619509; project E2SWITCH) and the BMBF project UltraLowPow (16ES0060 K).

[1] S. Wirths, R. Geiger, N. von den Driesch, G. Mussler, T. Stoica, S. Mantl, Z. Ikonic, M. Luysberg, S. Chiussi, J. M. Hartmann, H. Sigg, J. Faist, D. Buca, and D. Grützmacher, Nature Photonics **9**, 88 (2015).

[2] Y. Yang, G. Han, P. Guo, W. Wang, X. Gong, L. Wang, K. L. Low, and Y.-C. Yeo, Electron Devices, IEEE Transactions on **60**, 4048 (2013).

[3] S. Wirths, A. T. Tiedemann, Z. Ikonic, P. Harrison, B. Holländer, T. Stoica, G. Mussler, M. Myronov, J. M. Hartmann, D. Grützmacher, D. Buca, and S. Mantl, Applied Physics Letters **102**, 192103 (2013).

[4] Q. Smets, D. Verreck, A. S. Verhulst, R. Rooyackers, C. Merckling, M. Van De Put, E. Simoen, W. Vandervorst, N. Collaert, V. Y. Thean, B. Sorée, G. Groeseneken, and M. M. Heyns, Journal of Applied Physics **115** (2014), 10.1063/1.4875535.

[5] L. Esaki, Physical Review **109**, 603 (1958).

[6] M. Oehme, Thin Solid Films **520**, 3341 (2012).

[7] M. Oehme, A. Karmous, M. Sarlija, J. Werner, E. Kasper, and J. Schulze, Applied Physics Letters **97**, 012101 (2010).

[8] M. Stoffel, G. S. Kar, and O. G. Schmidt, Materials Science and Engineering C **25**, 826 (2005).

[9] M. T. Björk, H. Schmid, C. D. Bessire, K. E. Moselund, H. Ghoneim, S. Karg, E. Lörtscher, and H. Riel, Applied Physics Letters **97**, 12 (2010).

[10] S. Gupta, B. Vincent, B. Yang, D. Lin, F. Gencarelli, J.-Y. J. Lin, R. Chen, O. Richard, H. Bender, B. Magyari-Köpe, M. Caymax, J. Dekoster, Y. Nishi, and K. C. Saraswat, in *Electron Devices Meeting (IEDM), 2012 IEEE International* (IEEE, 2012) pp. 16–2.

[11] G. Han, S. Su, C. Zhan, Q. Zhou, Y. Yang, L. Wang, P. Guo, W. Wei, C. P. Wong, Z. X. Shen, B. Cheng, and Y.-C. Yeo, in *Electron Devices Meeting (IEDM), 2011 IEEE International* (IEEE, 2011) pp. 16–7.

[12] Y. Yang, K. Lu Low, W. Wang, P. Guo, L. Wang, G. Han, and Y.-C. Yeo, Journal of Applied Physics **113**, 194507 (2013).

[13] C. Eckhardt, K. Hummer, and G. Kresse, Physical Review B **89**, 165201 (2014).

[14] K. Lu Low, Y. Yang, G. Han, W. Fan, and Y.-C. Yeo, Journal of Applied Physics **112**, 103715 (2012).

[15] T. B. Bahder, Physical Review B **41**, 11992 (1990).

[16] S. Wirths, Z. Ikonic, A. T. Tiedemann, B. Holländer, T. Stoica, G. Mussler, U. Breuer, J. M. Hartmann, a. Benedetti, S. Chiussi, D. Grützmacher, S. Mantl, and D. Buca, Applied Physics Letters **103**, 192110 (2013).

[17] Y. Bogumilowicz and J. M. Hartmann, Thin Solid Films **557**, 4 (2014).

[18] S. Wirths, R. Troitsch, G. Mussler, J.-M. Hartmann, P. Zaumseil, T. Schroeder, S. Mantl, and D. Buca, Semiconductor Science and Technology **30**, 055003 (2015).